Proc. NIPR Symp. Polar Meteorol. Glaciol., 7, 41–50, 1993

A PRELIMINARY STUDY ON GEOSAT ALTIMETER OBSERVATION IN THE SOUTHERN OCEAN

Takashi KIKUCHI[1], Akira SHIBATA[2] and Masaaki WAKATSUCHI[1]

[1]*Institute of Low Temperature Science, Hokkaido University, Kita-19, Nishi-8, Kita-ku, Sapporo 060*
[2]*Meteorological Research Institute, 1–1, Nagamine, Tsukuba 305*

Abstract: The Geosat sea-level anomaly in the Southern Ocean south of 30°S in the period from November 1986 to December 1987 is calculated by applying the collinear method to retrieve sea-level from the Geosat altimeter data. The Geosat sea-level data are used to investigate the variation and time-dependency in sea-level anomaly in the Southern Ocean.

Regions with high variability in sea-level anomaly correspond to the confluence zones of subtropical and subantarctic water and to the Antarctic Circumpolar Current(ACC). Two regions with higher variability exist in the ACC. High variability south of New Zealand is closely related to the bottom topography. The sea-level anomaly in this region does not show a clear propagation signal, while the strong anomaly generated in Drake Passage propagates down stream at a speed of 4.5 cm/s. In the southern regions of the ACC we were not able to find any significant variation of the Geosat sea-level data. Time-dependency of sea-level variation along a latitude of 40°S suggests that the Agulhas eddies are generated near 30°S and move westward at a speed of 10–15 cm/s.

1. Introduction

The U.S. Navy Geodetic Satellite, also called Geosat, was launched on March 1985. On board is a 13.5 GHz radar altimeter with precision of about 3.5 cm in height measurement. This altimeter provides a variety of geophysical data, such as sea-level variability, significant wave height, surface wind speed and so on.

A preliminary mission of the Geosat, also called the Geodetic Mission (GM), was precise measurement of marine gravity field, which ended in September 1986. Then the Geosat was maneuvered into a 17-day exact repeat orbit to begin another mission called the Exact Repeat Mission (ERM). The ERM ground-tracks were designed to repeat 244 orbital resolutions with the exact repeat cycle of 17.05 days. The ERM data became operational on November 8, 1986. Under an agreement with the U.S. Navy and in collaboration with the Applied Physics Laboratory of Johns Hopkins University, the National Oceanographic Data Center of NOAA distributes the Geosat ERM Geophysical Data Records (GDRs). The GDRs contain several geophysical data to retrieve sea-level from the altimeter data, such as corrections of solid earth tide, surface ocean tide, wet troposphere, dry troposphere and ionosphere (CHENEY *et al.*, 1987).

The Geosat ERM ground-tracks cover the area between 72°N and 72°S. CHELTON *et al.* (1990) have investigated the large-scale, low-frequency variability in sea-level and surface geostrophic velocity in the Southern Ocean using the Geosat altimeter data. Several investigators (WAKKER *et al.*, 1990; GORDON and HAXBY, 1990; FERON *et al.*, 1992) have studied some regional oceanic features (*e.g.* the Agulhas Retroflection and the associated ring-shedding process).

In this paper, we present Geosat sea-level variability in the Southern Ocean south of 30°S. In the next section we show a method of obtaining a sea-level anomaly data-set from the Geosat altimeter data. In Section 3 we present the observational results of the Geosat sea-level variability. Time-dependencies of sea-level anomaly are used to examine characteristics of sea-level anomaly in the Southern Ocean south of 30°S. Finally, we summarize our results in Section 4.

2. Geosat Altimeter Data

The Geosat ERM altimeter data during the period from November 1986 to December 1987 (*i.e.* 24 repeat cycles of Geosat) are incorporated in this study. Figure 1 shows the Geosat ground-tracks used in this study. The ground-tracks of the Geosat are chosen in the Southern Ocean south of 30°S. The southern limit of the Geosat ground-tracks is at the Antarctic continent or sea ice edge. ERM cycle data along the ascending tracks are often defecting in high latitude. Therefore, such data are not used.

Our method for retrieving sea-level from the Geosat altimeter data is as follows. Errors caused by tidal and atmospheric effects are eliminated from the initial Geosat altimeter data. We use the geophysical data contained in the

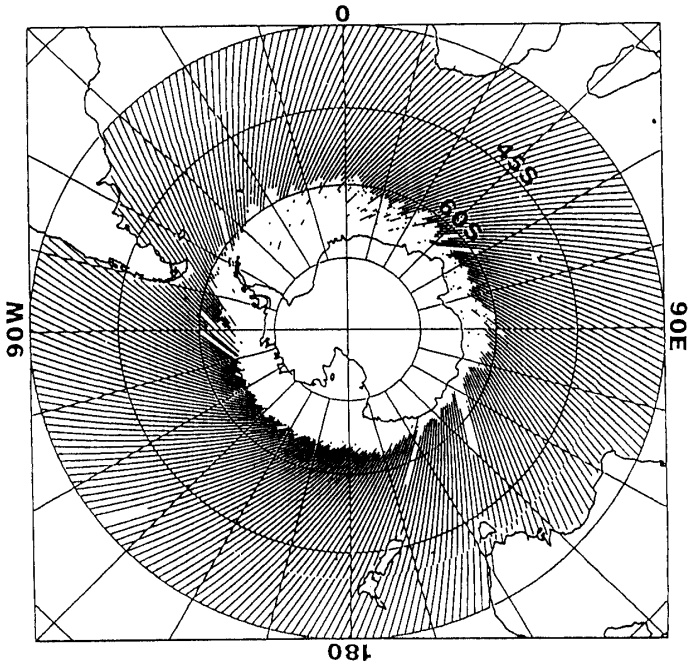

Fig. 1. A map of the Geosat ground-tracks used in this study.

GDRs as the values of tidal and atmospheric errors. However the data still include both the marine geoid and the orbit error. To remove these effects we use the collinear method (SHIBATA and KITAMURA, 1990). Since the marine geoid is time-invariant and has a dynamical range much larger than the sea surface topography associated with ocean current, the geoid effect is eliminated by removing the mean sea-level of 24 repeat cycles of data from each cycle of data. Therefore, the calculated Geosat sea-level does not have any information about the mean sea-level. Orbit error also has dynamical range much larger than the oceanic signal. This error can be estimated by a least-square curve fit. The use of a high-order least-square curve removes oceanic signals, but the use of a low-order one leads to large residual errors. In this study, we use a least-square curve of second order. Then the orbit error is eliminated by removing the estimated least-square fitting curve from the Geosat data profiles along each track.

Figure 2 shows a map of the standard deviation of the Geosat sea-level anomaly computed from the data along each ground-track. For convenience, the Geosat data along all tracks are reduced to gridded data. In this study, gridpoints are at 1 degree interval. Gridded data between 31°S and 55°S are used. In the Weddell Sea region, however, southern limits move northward. Since Antarctic sea ice extends to 55°S north of the Weddell Sea in winter (ZWALLY *et al.*, 1983),

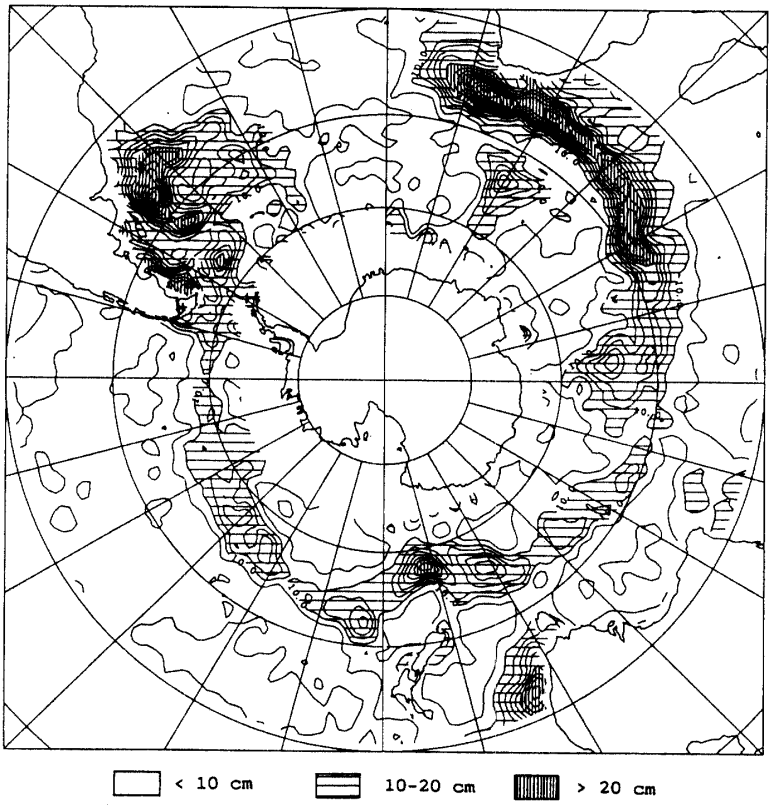

Fig. 2. The standard deviation calculated from the Geosat sea-level anomaly data along each ground-track. The contour interval is 2 cm.

Geosat sea-level data were lacking in this region (see Fig. 1). The detail of the gridding procedure is as follows. A scheme of the iterative difference-correction type (CRESSMAN, 1959; LEVITUS, 1982) is used to compute the 1° gridded data. The gridpoints are chosen at intersections of latitude and longitude lines. At all gridpoints the first-guess field is computed as a distance-weighted mean of the track data within the area of an influence radius. We choose 200 km as the influence radius. A Gaussian function is applied as a weight function. If there are no data within the area of the influence radius or the data exist only on one side of the gridpoint, the gridpoint data are not defined. A final-guess field is computed as a distance-weighted mean of the first-guess gridded data with the same function and influence radius for each gridpoint again.

3. Results

As shown in Fig. 2, there are several high variability regions. For example, the highest variability is indicated in a region south of Africa (more than 36 cm). Figure 3 shows geopotential anomaly relative to 1500 db. Note that regions with

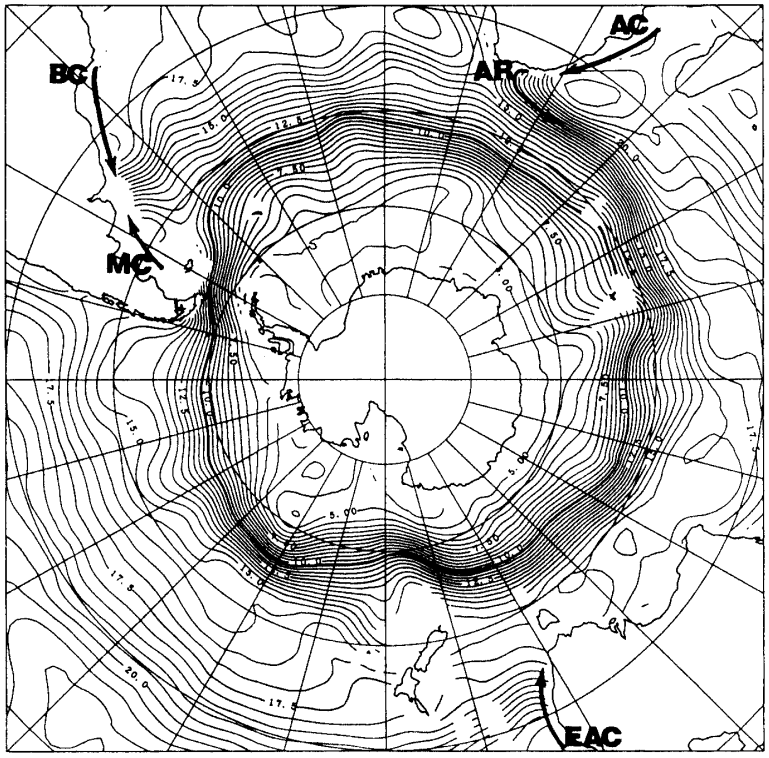

Fig. 3. The 0/1500 db geopotential anomaly calculated from the LEVITUS (1982) annual mean hydrographic data. The contour interval is 0.5 m^2/s^2. The thick line is the 10.5 m^2/s^2 geopotential anomaly line. This line represents the axis of the Antarctic Circumpolar Current. Each arrow in this figure shows the current: The Agulhas Current (AC), the Agulhas Retroflection (AR), the Brazil Current (BC), the Malvinas Current (MC) and the East Australia Current (EAC).

high variability are closely related to strong gradient of geopotential anomaly. In the Southern Ocean, these regions can be divided into the two types. One is due to the confluence of subtropical and subantarctic water masses. The other is caused by the ACC.

The Pacific, the Atlantic and the Indian Ocean have regions with high variability, which are due to the confluence of subtropical and subantarctic waters. In the Pacific Ocean, the East Australia Current carries subtropical water to the western Tasman Sea. As shown in Figs. 2 and 3, the western Tasman Sea has high variability and strong gradient of geopotential anomaly. The poleward Brazil current and the equatorward Malvinas current meet near the 35°–40°S along the South American continent. This confluence also has high variability and strong geopotential gradient. In this region, the shape of the high variability region reflects the effect of the bottom topography (GORDON and HAXBY, 1990; CHELTON *et al.*, 1990). In the region south of Africa, the Agulhas current, which is the western boundary current in the Indian Ocean, retroflects and flows eastward as the Agulhas Return current (Fig. 3). On the western side of the Agulhas Retroflection, Agulhas Ring-shedding occurs. These current systems cause high variability of sea-level anomaly. We will show details of the sea-level variation south of Africa later on.

As shown in Figs. 2 and 3, the ACC generally has high variability. In particular, regions with high variability exist south of New Zealand (around 58°S, 170°E) and downstream from Drake Passage (from 55°S, 60°W to 48°S, 30°W). In these regions, there is a strong gradient of geopotential anomaly and the width of the ACC is narrower than that in other regions. The ACC seems to exist as a banded structure, with multiple narrow jets associated with a strong lateral density gradient at the subantarctic and polar fronts. The positions of these fronts are highly variable and excursions of up to 100 km in 10 days have been observed (NOWLIN and KLINCK, 1986). The meander can lead to the formation of eddies and current rings (JOYCE *et al.*, 1981). The variability of Geosat sea-level corresponds to these phenomena.

To investigate the variation in sea-level anomaly, we examine the time-dependency of the Geosat sea-level anomaly. First, we consider the time-dependency of sea-level anomaly along the ACC. The lines of 10.5 m^2/s^2 in geopotential anomaly, calculated from the LEVITUS (1982) hydrographic data set, are used as the position of the ACC, as shown in Fig. 3. Figure 4 shows the time-dependency of the Geosat sea-level anomaly along the line of 10.5 m^2/s^2 in geopotential anomaly. It seems that there is no distinct zonal coherence in sea-level variability except for a region downstream from the Drake Passage.

The ACC has two regions with higher variability, as shown in Fig. 2. South of New Zealand high variability is confined within 155°–170°E. This variability is closely related to the bottom topography, and does not have a clear propagation signal in sea-level anomaly. In this region there also seems to be seasonal variation. Positive anomaly in sea-level is dominant during the period from November 1986 to May 1987, while negative anomaly is dominant from June 1987 to December 1987. It is not clear why the seasonal variation is found only

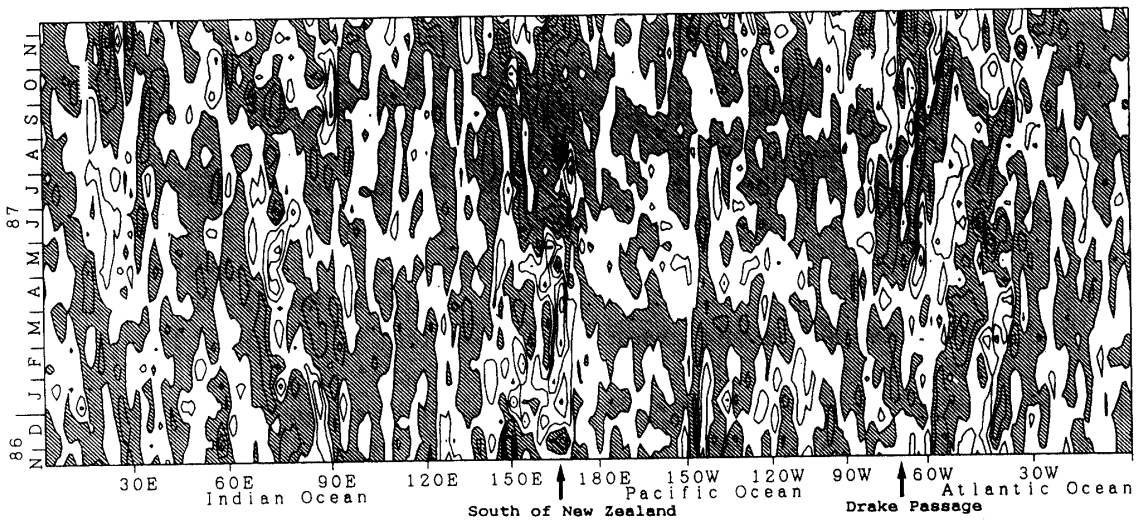

Fig. 4. The time-longitude dependency in sea-level anomaly along the line of 10.5 m^2/s^2 in geopotential anomaly. The contour interval is 5 cm. Hatched regions indicate the negative sea level anomaly.

in this region. The sea-level anomaly east of Drake Passage (about 70°W) shows eastward propagation at a speed of about 4.5 cm/s. This propagation starts at Drake Passage and reaches 40°W. Eddy formation near the Drake Passage has been observed by several investigators (GORDON *et al.*, 1977; JOYCE *et al.*, 1981). Several numerical studies indicate that the eddies are generated by baroclinic instability of the mean flow (MCWILLIAMS *et al.*, 1978; TREGUIER and MCWILLIAMS, 1990). The time-dependency of the Geosat sea-level anomaly along the ACC indicates that eddy-like features generated in the Drake Passage propagate downstream at a speed of about 4.5 cm/s.

In Figs. 5a–d, the time-longitude dependency is shown for the latitudes of 34°S, 40°S, 50°S and 60°S, respectively. The line along 34°S is chosen to see the subtropical gyre. Figure 5a indicates that sea-level anomaly propagates westward at an average speed of about 10.0 cm/s in the subtropical gyre. The 40°S line (Fig. 5b) contains the confluence of subtropical and subantarctic waters. High variability is found east of South America (62°–35°W) and around South Africa (15°–55°E). The region around South Africa can be divided into two domains according to propagation velocity. In the western domain (15°–30°E) the sea-level anomaly moves westward at a speed much faster than that in the eastern domain (30°–55°E). The speed is 10–15 cm/s in the western domain, while it is 0–2 cm/s in the eastern domain.

Figure 6 shows the Geosat sea-level anomaly south of Africa. It is clear that the positive anomaly labeled A moves westward. On the other hand, the negative anomaly labeled B in the eastern domain is stationary or moves westward slightly. Anomaly A corresponds to the Agulhas eddy and anomaly B corresponds to the meandering of the Agulhas Retroflection. The Agulhas eddies have been studied by several researchers (BOUDRA and CHASSIGNET, 1988; LUTJEHARM and BALLEGOOYEN, 1988; GORDON and HAXBY, 1990; FERON *et al.*, 1992). Figure 5b indicates that the Agulhas eddies are generated near 30°E and move

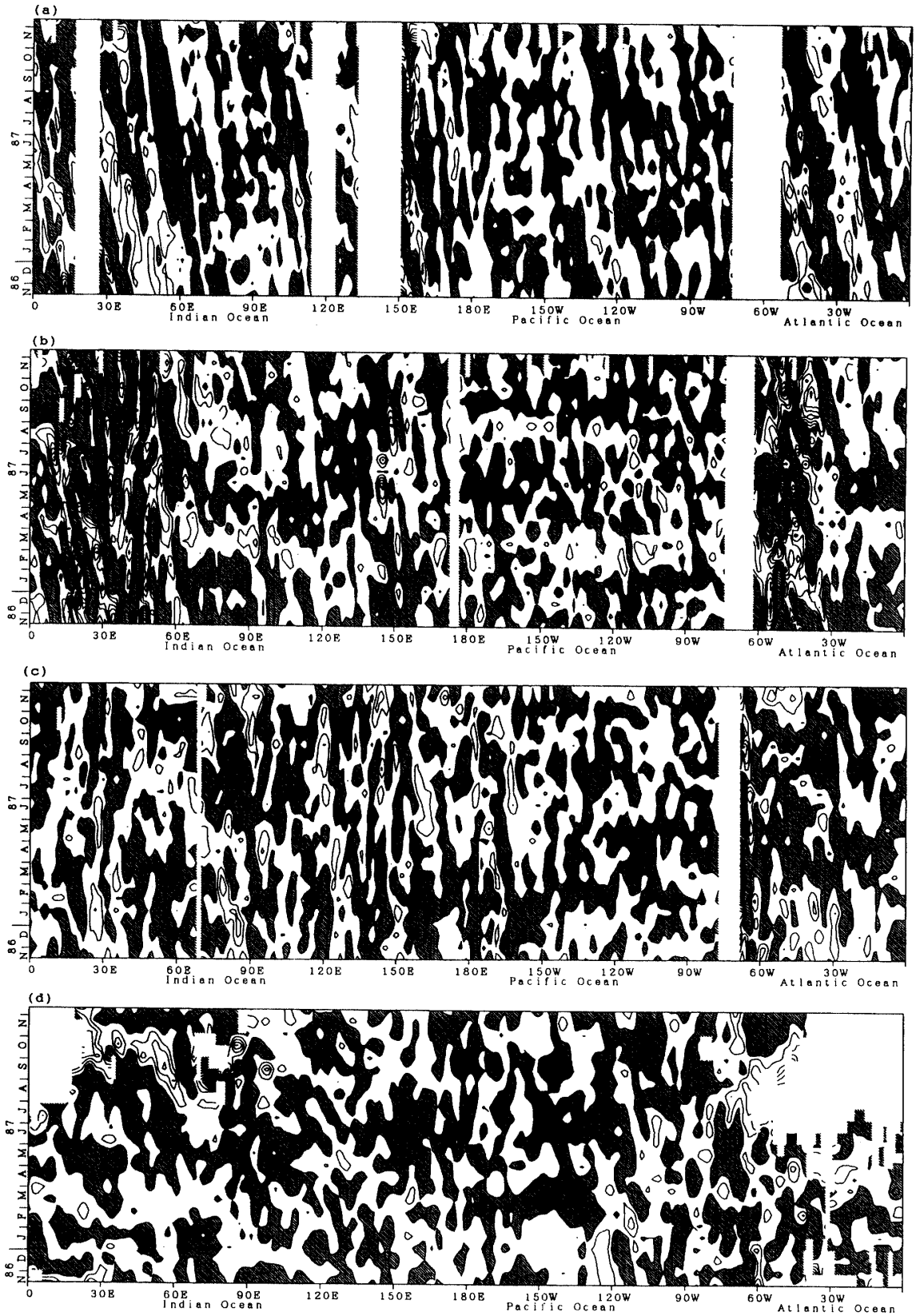

Fig. 5. The time-longitude dependency in sea-level anomaly at (a) 34°S, (b) 40°S, (c) 50°S and (d) 60°S. The contour interval is 5 cm. Hatched regions indicate the negative sea-level anomaly.

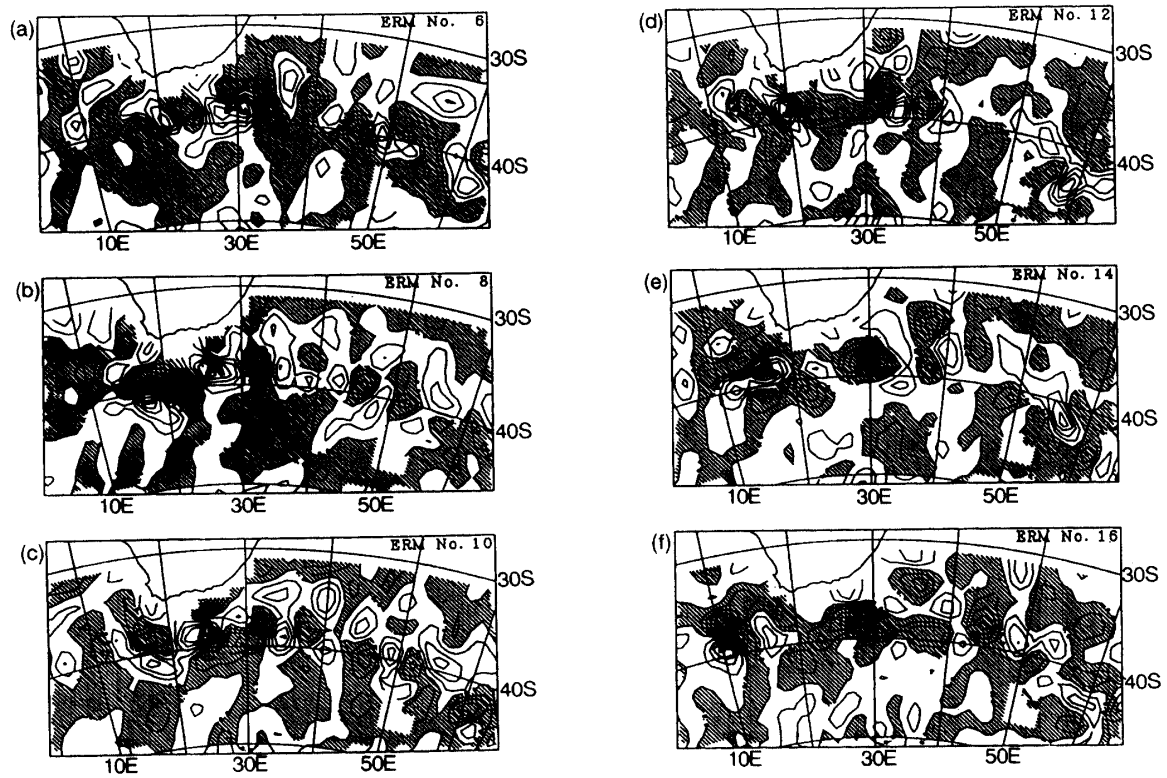

Fig. 6. Maps of the Geosat sea-level anomaly south of Africa during (a) ERM No. 6 (1987.2.1–2.17), (b) ERM No. 8 (1987.3.7–3.23), (c) ERM No. 10 (1987.4.10–4.26), (d) ERM No. 12 (1987.5.14–5.30), (e) ERM No. 14 (1987.6.17–7.3) and (f) ERM No. 16 (1987.7.21–8.6). The contour interval is 5 cm. Hatched regions indicate negative sea-level anomaly. West of 30°E, the positive anomaly marked A moves westward. East of 30°E, the negative anomaly marked B is nearly stationaly.

westward at a speed of 10–15 cm/s.

Figure 5c contains the variability caused by the ACC (90°–150°E and 45°–30°W). Figure 5d shows the sea-level anomaly in a region south of the ACC. In the regions we cannot find any significant variation. Note that anomalies shown in both Figs. 5c and 5d are very weak except near the ACC (see Fig. 2). Since density stratification is very weak in the polar region, baroclinic flow, accordingly the surface velocity, seems to be small. This may explain why sea-level variability south of the ACC is very small.

4. Summary

The Geosat sea-level anomaly in the Southern Ocean south of 30°S in the period from November 1986 to December 1987 is calculated from the Geosat altimeter data applying the collinear method to retrieve sea-level. The summary of this study is as follows.

(1) In the Southern Ocean south of 30°S, the regions of high standard deviation in Geosat sea-level are closely related to strong gradient of geopotential anomaly. High variability regions correspond to confluence zones of subtropical

and subantarctic water and to the ACC. Westward propagation of anomaly is found in the subtropical region. South of the ACC there is no significant variability.

(2) The ACC has two regions with higher variability in sea-level anomaly, which are found south of New Zealand and downstream from Drake Passage. Variations in the region south of New Zealand are closely related to the bottom topography. The sea-level anomaly in this region does not show a clear propagation signal, while the strong anomalies generated in Drake Passage propagate downstream at a speed of 4.5 cm/s.

(3) The region south of Africa has the highest variability in the Southern Ocean. The Geosat sea-level anomaly data show that Agulhas eddies are generated near 30 and move westward at a speed of 10–15 cm/s.

Acknowledgments

We are much indebted to Dr. K. I. OHSHIMA and Dr. Y. FUKAMACHI for their valuable comments and suggestions. This work was partly supported by Grant-in-Aid No. 03452059 for Scientific Research from the Ministry of Education, Science and Culture of Japan.

References

BOUDRA, D. B. and CHASSIGNET, E. P. (1988): The dynamics of Agulhas Retroflection and ring formation in a numerical model, I, The vorticity balance. J. Phys. Oceanogr., **18**, 280–303.

CHELTON, D. B., SHCLAX, M. G., WITTER, D. L. and RICHMAN, J. G. (1990): Geosat altimeter observation of the surface circulation of the Southern Ocean. J. Geophys. Res., **95**, 17877–17903.

CHENEY, R. E., DOUGLAS, B. C., AGREEN, R. W., MILLER, L., PORTER, D. L. and DOYLE, N. S. (1987): Geosat Altimeter Gophysical Data Record User Handbook. NOAA Tech. Memo. NOS NG-**46** 32p.

CRESSMAN, G. P. (1959): An operational objective analysis scheme. Mon. Weather Rev., **87**, 329–340.

FERON, R. C. V., DE RUIJTER, W. P. M. and OSKAM, D. (1992): Ring shedding in the Agulhas Current System. J. Geophys. Res., **97**, 9467–9477.

GORDON, A. L. and HAXBY, W. F. (1990): Agulhas eddies invade the South Atlantic: Evidence from Geosat altimeter and shipboard conductivity-temperature-depth survey. J. Geophys. Res., **95**, 3117–3125.

GORDON, A. L., GEORGI, D. T. and TAYLOR, H. W. (1977): Antarctic Polar Front zone in the western Scotia Sea. Summer 1975. J. Phys. Oceanogr., **7**, 309–328.

JOYCE, T. M., PATTERSON, S.L. and MILLARD, R. C., Jr. (1981): Anatomy of a cyclonic ring in the Drake Passage. Deep-Sea Res., **28**, 1265–1287.

LEVITUS, S. (1982): Climatological Atlas of the World Ocean. NOAA Prof. Pap. **13**.

LUTJEHARM, J. R. E. and VAN BALLEGOOYEN, R. C. (1988): The retroflection of the Agulhas Current. J. Phys. Oceanogr., **18**, 1570–1588.

MCWILLIAMS, J. C., HOLLAND, W. R. and CHOW, J. H. S. (1978): A description of numerical Antarctic Circumpolar Current. Dyn. Atmos. Oceans, **2**, 213–291.

NOWLIN W. D., Jr. and KLINCK, J. M. (1986): The physics of the Antarctic Circumpolar Current. Rev. Geophys., **24**, 469–491.

SHIBATA, A. and KITAMURA, Y. (1990): Geosat sea level variability in the Tropical Pacific in the period from November 1986 to February 1989, obtained by collinear method. Oceanogr. Mag., **40**, 1–26.

TREGUIER, A. M. and MCWILLIAMS, J. C. (1990): Topographic influences on wind-driven, stratified flow on a β-plane channel: An idealized model of the Antarctic Circumpolar Current. J. Phys. Oceanogr., **20**, 321–343.

WAKKER K. F., ZANDBERGEN, R. C. A., NAEIJE, M. C. and AMBROSIUS, B. A. C. (1990): Geosat altimeter data analysis for the ocean around South Africa. J. Geophys. Res., **95**, 2991–3006.

ZWALLY, H. J., COMISO, J. C., PARKINSON, C. L., CAMPBELL, W. J., CARSEY, F. D. and GLOERSON, P. (1983): Antarctic Sea Ice, 1973–1976: Satellite Passive-Microwave Observation. Washington, D.C., NASA, 206 p. (NASA SP-459).

(Received November 8, 1992; Revised manuscript received April 2, 1993)